14th International Conference on Information Fusion
Chicago, Illinois, USA, July 5-8, 2011

Shooter Localization using Soldier-Worn Gunfire Detection Systems

Jemin George and Lance M. Kaplan
{jemin.george & lance.m.kaplan}@us.army.mil
U.S. Army Research Laboratory, Adelphi, MD 20783-1197

***Abstract*—This paper considers the problem of shooter localization using a network of soldier-worn gunfire detection systems. Proposed scheme utilizes the benefits of sensor network layout of all the sensors within a small combat unit to help refine localization accuracy. If the soldier is within the field of view of the shockwave, then using the acoustic phenomena analysis of small-arms fire, the gunfire detection system can localize the source of the incoming fire and the bullet's trajectory with respect to the sensor location. These individual solutions, usually in the form of a bearing and range relative to the soldier, are then relayed to the central node. At the central node level, the individual solutions are fused along with the GPS locations on the soldiers to yield a highly accurate geo-rectified solution.**

Keywords: Shooter localization, gunfire detection system, maximum likelihood estimation, Gauss-Newton method.

I. Introduction

There is an eminent need for highly accurate small-arms gunfire detection systems on individual soldiers for added battlefield situational awareness and threat assessment. Today, several acoustic shooter localization systems are commercially available [1], [2]; an overview of such systems can be found in [3]. Currently operational Soldier Wearable Gunfire Detection Systems (SW-GDSs) can provide an appropriate level of localization accuracy as long as the soldier is at an ideal location (range, attitude, etc.) when incoming fire is received [4]–[6]. The localization system suffers severe performance degradation when the soldier is at a non-ideal location. Moreover, when a relative solution, i.e., the shooter location relative to the sensor, is transformed into a geo-rectified solution using a magnetometer and GPS, the solution often becomes unusable due to localization errors. Geo-rectified solutions are necessary when displaying hostile fire icons on a Command and Control Geographic Information System (C2 GIS) map display.

SW-GDSs use acoustic phenomena analysis of small-arms fire to localize the source of incoming fire, usually with a bearing and range relative to the user [7]. These individual SW-GDSs operate separately and are not designed to exploit the sensor network layout of all the soldiers within a Small Combat Unit (SCU) to help increase accuracy. Researchers are exploring some novel solutions that utilize the team aspect of these SCUs by exploiting all SW-GDSs in a squad/platoon to increase detection rates and accuracy [8]–[10]. This paper presents the development of a sensor fusion module that would take full advantage of the team aspect of a SCU to provide a fused solution that would be highly accurate and suitable for a C2 GIS map display compared to the individual soldier's solution. The objective here is to improve accuracy across an entire SCU so even soldiers in non-ideal settings (out of range, bad angle, etc.) can exploit the good solutions from their neighbors to come up with improved solutions: both geo-rectified and relative.

The individual SW-GDSs considered here is composed of a passive array of microphones that is able to localize a gunfire event by measuring the direction of arrival for both the acoustic wave generated by the muzzle blast and the shockwave generated by the supersonic bullet [1], [2]. After detecting a gunfire, the individual sensors report their solution along with their GPS positions to a central node. At the central node, the individual solutions are fused along with the GPS positions to yield an highly accurate, geo-rectified solution, which is then relayed back to individual soldiers for added situational awareness. Structure of this paper is as follows: section II presents the measurement model for the acoustic sensor nodes, and section III presents the localization algorithm that converts the sensor measurements to a gunfire position estimate. Details of the central node data fusion and the corresponding nonlinear least-squares problem is given in section IV. Section V presents the Gauss-Newton method to solve the nonlinear least-squares problem and section VI presents the results from numerical simulations. Finally, section VII concludes the paper and discusses the current research challenges.

II. Problem Setup

Consider a SCU consist of n individual soldiers equipped with the SW-GDS. In order to set up the problem and develop a sensor model, we first consider a scenario where there is only one shooter and the SW-GDS receives both the muzzle blast and the shockwave. The shooter or the target location and the soldier or the i^{th} sensor location are defined as T and S_i, respectively. For simplicity, the problem is formulated in $\Re^2$, i.e., $T \in \Re^2 \equiv \begin{bmatrix} T_x \\ T_y \end{bmatrix}$ and $S_i \in \Re^2 \equiv \begin{bmatrix} S_{i_x} \\ S_{i_y} \end{bmatrix}$. Now define the individual range, r_i, and bearing, ϕ_i, between the i^{th} sensor node and the target as

$$r_i = \sqrt{\left(T_x - S_{i_x}\right)^2 + \left(T_y - S_{i_y}\right)^2} \tag{1}$$

$$\phi_i = \arctan 2\left(T_y - S_{i_y}, T_x - S_{i_x}\right) \tag{2}$$

Report Documentation Page

Form Approved
OMB No. 0704-0188

1. REPORT DATE	2. REPORT TYPE	3. DATES COVERED
JUL 2011		**00-00-2011 to 00-00-2011**

4. TITLE AND SUBTITLE	5a. CONTRACT NUMBER
Shooter Localization using Soldier-Worn Gunfire Detection Systems	5b. GRANT NUMBER
	5c. PROGRAM ELEMENT NUMBER
6. AUTHOR(S)	5d. PROJECT NUMBER
	5e. TASK NUMBER
	5f. WORK UNIT NUMBER
7. PERFORMING ORGANIZATION NAME(S) AND ADDRESS(ES) **U.S. Army Research Laboratory,Adelphi,MD,20783-1197**	8. PERFORMING ORGANIZATION REPORT NUMBER
9. SPONSORING/MONITORING AGENCY NAME(S) AND ADDRESS(ES)	10. SPONSOR/MONITOR'S ACRONYM(S)
	11. SPONSOR/MONITOR'S REPORT NUMBER(S)

12. DISTRIBUTION/AVAILABILITY STATEMENT
Approved for public release; distribution unlimited

13. SUPPLEMENTARY NOTES
Presented at the 14th International Conference on Information Fusion held in Chicago, IL on 5-8 July 2011. Sponsored in part by Office of Naval Research and U.S. Army Research Laboratory.

14. ABSTRACT
This paper considers the problem of shooter localization using a network of soldier-worn gunfire detection systems. Proposed scheme utilizes the benefits of sensor network layout of all the sensors within a small combat unit to help refine localization accuracy. If the soldier is within the field of view of the shockwave, then using the acoustic phenomena analysis of small-arms fire, the gunfire detection system can localize the source of the incoming fire and the bullet?s trajectory with respect to the sensor location. These individual solutions, usually in the form of a bearing and range relative to the soldier, are then relayed to the central node. At the central node level, the individual solutions are fused along with the GPS locations on the soldiers to yield a highly accurate geo-rectified solution.

15. SUBJECT TERMS

16. SECURITY CLASSIFICATION OF:			17. LIMITATION OF ABSTRACT	18. NUMBER OF PAGES	19a. NAME OF RESPONSIBLE PERSON
a. REPORT **unclassified**	b. ABSTRACT **unclassified**	c. THIS PAGE **unclassified**	**Same as Report (SAR)**	**8**	

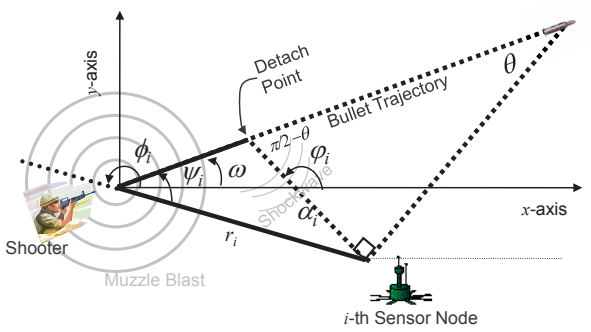

Figure 1. Geometry of the bullet trajectory and propagation of the muzzle blast and shockwave to the sensor node.

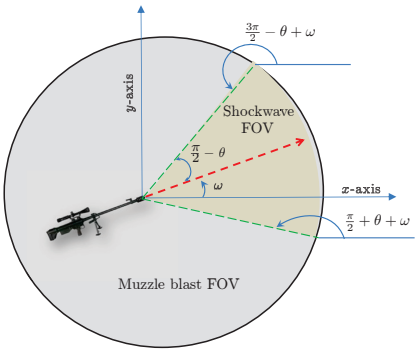

Figure 2. Muzzle blast and shockwave field of view

When a gun fires, the blast from the muzzle produces a spherical acoustic wave that can be heard in any direction. The bullet travels at supersonic speeds and produces an acoustic shockwave that emanates as a cone from the trajectory of the bullet. Because the bullet is traveling faster than the speed of sound, the shockwave arrives at the sensor node before the wave from the muzzle blast, which we simply refer to as the muzzle blast. Figure 1 illustrates the geometry of the shockwave and the muzzle blast for the i^{th} sensor node when the orientation of the bullet trajectory is ω with respect to the horizontal axis. As the bullet pushes air, it creates an impulse wave. The wavefront is a cone whose angle θ with respect to the trajectory is

$$\theta = \arcsin\left(\frac{1}{m}\right) \tag{3}$$

where m is the Mach number. The Mach number is assumed to be known since the typical value for a Mach number is $m = 2$ [7]. Since the Mach number directly influences the range estimates, uncertainty in bullet speed may be treated as range estimation error. As indicated in figure 1, the angle ϕ_i indicates the direction of arrival (DOA) of the muzzle blast, and φ_i indicates the DOA of the shockwave. The muzzle blast DOA is measured counter-clockwise such that $0 \leq \phi_i \leq 2\pi$[1]. For a more detailed description of the scenario, please refer to [7]. Figure 2 indicates the field of view (FOV) for both the muzzle blast and the shockwave. Note that the FOV of the muzzle blast is 2π, i.e., omnidirectional, and the FOV for the shockwave is $\pi - 2\theta$. SW-GDS receives the shockwave only if the muzzle blast DOA is within the bounds

$$\pi/2 + \theta + \omega < \phi_i < 3\pi/2 - \theta + \omega \tag{4}$$

Now the DOA angle for the shockwave can be written as

$$\varphi_i = \begin{cases} -\frac{\pi}{2} - \theta + \omega, & \text{if } \pi + \omega < \phi_i < \frac{3\pi}{2} - \theta + \omega; \\ \frac{\pi}{2} + \theta + \omega, & \text{if } \frac{\pi}{2} + \theta + \omega < \phi_i < \pi + \omega. \end{cases} \tag{5}$$

The first case $\pi + \omega < \phi_i < \frac{3\pi}{2} - \theta + \omega$ corresponds to the scenario where the sensor is located above the bullet trajectory and the third case $\frac{\pi}{2} + \theta + \omega < \phi_i < \pi + \omega$ corresponds to the scenario where the sensor is located below the bullet trajectory (as shown in figure 1). The case where $\phi_i = \pi + \omega$ corresponds to the scenario when the sensor is located on the bullet trajectory and here we do not consider such a scenario.

If ϕ_i is outside the bound given in (4), the sensor node only receives the the muzzle blast and it is outside the FOV of the shockwave. Under the assumptions that the bullet maintains a constant velocity over its trajectory, the time difference between the shockwave and the muzzle blast can be written as [2]

$$\tau_i = \frac{r_i}{c}\left[1 - \cos|\phi_i - \varphi_i|\right], \quad \forall \phi_i \neq \varphi_i \tag{6}$$

where c indicates the speed of sound. Utilizing (5), the bullet trajectory angle, ω, can be obtained from the shockwave DOA angle. Though this paper assumes that the bullet speed is constant over its trajectory, others have proposed localization algorithms [10], [11] that employ more realistic bullet speed models at the expense of computational efficiency.

III. Data Fusion at Sensor Node Level

When the sensor node is within the FOV of the shockwave, the three available measurements are the two DOA angles and the time difference of arrival (TDOA) between the muzzle blast and the shockwave, i.e.,

$$\hat{\phi}_i = h_1(T, S_i, \omega) + \eta_\phi \tag{7}$$

$$\hat{\varphi}_i = h_2(T, S_i, \omega) + \eta_\varphi \tag{8}$$

$$\hat{\tau}_i = h_3(T, S_i, \omega) + \eta_\tau \tag{9}$$

where $h_1(\cdot)$ is given in (2), $h_2(\cdot)$ is given in (5), and $h_3(\cdot)$ is given in (6). The measurement noise is assumed to be zero mean Gaussian white noise, i.e., $\eta_\phi \sim \mathcal{N}(0, \sigma_\phi^2)$, $\eta_\varphi \sim \mathcal{N}(0, \sigma_\varphi^2)$ and $\eta_\tau \sim \mathcal{N}(0, \sigma_\tau^2)$. Let $\widehat{T}_i = \begin{bmatrix}\hat{\phi}_i & \hat{r}_i & \hat{\omega}_i\end{bmatrix}$ denotes the individual sensor level estimates on the target bearing, range, and the bullet trajectory. Data fusion at the sensor node involves calculating these individual estimates based on the three sensor measurements.

Using (5), the bullet trajectory angle, ω, can be obtained from the shockwave DOA measurements. Thus, the observations on the trajectory angle can be written as

$$\hat{\omega}_i = \omega_i + \eta_\varphi \tag{10}$$

[1]The $\arctan 2$ in (2) yields $-\pi \leq \phi_i \leq \pi$. Thus 2π must be added to the $\arctan 2$ result to obtain a positive ϕ_i if $\phi_i < 0$.

Now the likelihood function, $p\left(\hat{\omega}_i|T,S_i,\omega\right)$, can be written as

$$p\left(\hat{\omega}_i|T,S_i,\omega\right)=\mathcal{N}\left(\omega,\sigma_\varphi^2\right)$$

From (6), the range can be written in terms of the TDOA as

$$r_i=\frac{c\tau_i}{[1-\cos|\phi_i-\varphi_i|]} \tag{11}$$

The observation of r_i may be written as

$$\hat{r}_i=\frac{c\hat{\tau}_i}{\left[1-\cos\left|\hat{\phi}_i-\hat{\varphi}_i\right|\right]} \tag{12}$$

Using the first-order Taylor series, the range measurement can be approximated as

$$\begin{aligned}\hat{r}_i \approx & \frac{c\tau_i}{[1-\cos|\phi_i-\varphi_i|]} \quad + \\ & \left[\frac{c}{[1-\cos|\phi_i-\varphi_i|]} \quad -\frac{c\tau_i\sin|\phi_i-\varphi_i|}{[1-\cos|\phi_i-\varphi_i|]^2}\right]\begin{bmatrix}\eta_\tau\\ \eta_{\phi\varphi}\end{bmatrix} \\ & = r_i+H(T,S_i,\omega)\eta_r\end{aligned}$$

where

$$\eta_r=\begin{bmatrix}\eta_\tau\\ \eta_{\phi\varphi}\end{bmatrix} \quad \& \quad \eta_{\phi\varphi}\sim\mathcal{N}\left(0,\sigma_\phi^2+\sigma_\varphi^2\right)$$

and

$$H(T,S_i,\omega)=\left[\frac{c}{[1-\cos|\phi_i-\varphi_i|]} \quad -\frac{c\tau_i\sin|\phi_i-\varphi_i|}{[1-\cos|\phi_i-\varphi_i|]^2}\right]$$

Now the likelihood $p\left(\hat{r}_i|T,S_i,\omega\right)$ can be approximated as

$$p\left(\hat{r}_i|T,S_i,\omega\right)\approx\mathcal{N}\left(r_i,\sigma_r^2(T,S_i,\omega)\right)$$

where the variance $\sigma_r^2(T,S_i,\omega)$ can be written as

$$\sigma_r^2(T,S_i,\omega)=H(T,S_i,\omega)\begin{bmatrix}\sigma_\tau^2 & 0\\ 0 & \sigma_\phi^2+\sigma_\varphi^2\end{bmatrix}H^T(T,S_i,\omega) \tag{13}$$

Thus, the likelihood function $p\left(\widehat{T}_i|T,S_i,\omega\right)$ can be approximated as

$$p\left(\widehat{T}_i|T,S_i,\omega\right)\approx\mathcal{N}\left(\boldsymbol{\mu}_{T_i},\Sigma_{T_i}\right) \tag{14}$$

where

$$\boldsymbol{\mu}_{T_i}=\begin{bmatrix}\phi_i\\ r_i\\ \omega\end{bmatrix} \quad \& \quad \Sigma_{T_i}=\begin{bmatrix}\sigma_\phi^2 & 0 & 0\\ 0 & \sigma_r^2(T,S_i,\omega) & 0\\ 0 & 0 & \sigma_\varphi^2\end{bmatrix}$$

It is assumed that a GPS receiver is used to obtain an accurate positioning on each sensor. Thus, the position observation on the sensors are given as

$$\widehat{S}_i=\begin{bmatrix}S_{i_x}\\ S_{i_y}\end{bmatrix}+\begin{bmatrix}v_{i_x}\\ v_{i_y}\end{bmatrix} \tag{15}$$

where the noise terms are assumed to be zero mean Gaussian white, i.e., $v_{i_x}\sim\mathcal{N}(0,\sigma_{i_x}^2)$ and $v_{i_y}\sim\mathcal{N}(0,\sigma_{i_y}^2)$. Now the GPS measurement likelihood function may be written as

$$p\left(\widehat{S}_i|S_i\right)\sim\mathcal{N}\left(\begin{bmatrix}S_{i_x}\\ S_{i_y}\end{bmatrix},\begin{bmatrix}\sigma_{i_x}^2 & 0\\ 0 & \sigma_{i_y}^2\end{bmatrix}\right)\equiv\mathcal{N}\left(\boldsymbol{\mu}_{S_i},\Sigma_{S_i}\right) \tag{16}$$

Assumption 1. *Without loss of generality, it can be assumed that the GPS observations on sensor position are independent of target location, observations on target location, and the projectile trajectory information, i.e.,*

$$p\left(\widehat{S}_i|S_i\right)=p\left(\widehat{S}_i|T,S_i,\omega\right)=p\left(\widehat{S}_i|\widehat{T}_i,T,S_i,\omega\right)$$

Base on assumption 1, the joint probability $p\left(\widehat{T}_i,\widehat{S}_i|T,S_i,\omega\right)$ can be calculated as

$$p\left(\widehat{T}_i,\widehat{S}_i|T,S_i,\omega\right)=p\left(\widehat{S}_i|\widehat{T}_i,T,S_i,\omega\right)p\left(\widehat{T}_i|T,S_i,\omega\right) \tag{17}$$

Substituting (14) and (16), the above joint likelihood can be written as

$$p\left(\widehat{T}_i,\widehat{S}_i|T,S_i,\omega\right)\approx\mathcal{N}\left(\boldsymbol{\mu}_{S_i},\Sigma_{S_i}\right)\mathcal{N}\left(\boldsymbol{\mu}_{T_i},\Sigma_{T_i}\right) \tag{18}$$

Now using the Bayes' rule, the node level estimates are given as

$$p\left(T,S_i,\omega|\widehat{T}_i,\widehat{S}_i\right)=\frac{p\left(\widehat{T}_i,\widehat{S}_i|T,S_i,\omega\right)p\left(T,S_i,\omega\right)}{\int\int\int p\left(\widehat{T}_i,\widehat{S}_i|T,S_i,\omega\right)p\left(T,S_i,\omega\right)dTdS_id\omega} \tag{19}$$

Note that the denominator in (19) indicates the normalization factor and since no *a priori* information is assumed to be known, a uniform pdf may be selected for $p\left(T,S_i,\omega\right)$. Since the denominator is the normalizing term, which is a constant with respect to T, S_i, and ω, equation (19) can be written as

$$p\left(T,S_i,\omega|\widehat{T}_i,\widehat{S}_i\right)\approx\alpha p\left(\widehat{T}_i,\widehat{S}_i|T,S_i,\omega\right) \tag{20}$$

where α is a constant.

Now for a sensor located in the FOV of the shockwave, the target location can be estimated as:

$$\widehat{T}_{x_i}=\widehat{S}_{i_x}+\hat{r}_i\cos(\hat{\phi}_i) \tag{21}$$

$$\widehat{T}_{y_i}=\widehat{S}_{i_y}+\hat{r}_i\sin(\hat{\phi}_i) \tag{22}$$

When the sensor is located outside the shockwave FOV, the only estimate would be the bearing angle. After individual estimates are obtained at the sensor node level, the measured information is transmitted to a central node where it is fused to obtain a more accurate estimate of shooter location.

IV. Data Fusion at the Central Node

While sensors in the FOV of the muzzle blast and the shockwave yield a range, bearing, and trajectory angle estimates, the gunfire detection systems outside the FOV of the shockwave yield a muzzle blast DOA. Also, GPS measurements are available on each sensor locations. At the central node, this information from the individual sensor nodes is fused to obtain an accurate estimate of the shooter location, bullet trajectory angle, and the sensor location.

Based on assumption 1, the joint likelihood function associated with each sensor, i.e., $p\left(\widehat{T}_i, \widehat{S}_i | T, S_i, \omega\right)$, can be written as

$$p\left(\widehat{T}_i, \widehat{S}_i | T, S_i, \omega\right) = p\left(\widehat{S}_i | \widehat{T}_i, T, S_i, \omega\right) p\left(\widehat{T}_i | T, S_i, \omega\right)$$

Let $\mathbf{S}_{1:n} = \{S_1, S_2, \ldots, S_n\}$, $\widehat{\mathbf{T}}_{1:n} = \{\widehat{T}_1, \widehat{T}_2, \ldots, \widehat{T}_n\}$, and $\widehat{\mathbf{S}}_{1:n} = \{\widehat{S}_1, \widehat{S}_2, \ldots, \widehat{S}_n\}$, where n indicates the number of sensors. Since the sensor nodes are independent of each other, the joint conditional density $p\left(\widehat{\mathbf{T}}_{1:n}, \widehat{\mathbf{S}}_{1:n} | T, \mathbf{S}_{1:n}, \omega\right)$ can be defined as

$$p\left(\widehat{\mathbf{T}}_{1:n}, \widehat{\mathbf{S}}_{1:n} | T, \mathbf{S}_{1:n}, \omega\right) = \prod_1^n p\left(\widehat{T}_i, \widehat{S}_i | T, S_i, \omega\right) \quad (23)$$

Here we consider the maximum likelihood approach to obtain the fused estimates. In the maximum likelihood estimation approach considered here, an estimate of the sensor locations, the shooter location, and the bullet trajectory angle are obtained so that the joint log-likelihood function is maximized, i.e.,

$$\begin{aligned} \max_{T, \mathbf{S}_{1:n}, \omega} \quad & \ln\left\{p\left(\widehat{\mathbf{T}}_{1:n}, \widehat{\mathbf{S}}_{1:n} | T, \mathbf{S}_{1:n}, \omega\right)\right\} \\ \Rightarrow \max_{T, \mathbf{S}_{1:n}, \omega} \quad & \sum_1^n \ln\left\{p\left(\widehat{T}_i, \widehat{S}_i | T, S_i, \omega\right)\right\} \end{aligned} \quad (24)$$

Based on the results given in the previous section, the criteria for the maximum likelihood estimation can be written as

$$\max_{T, \mathbf{S}_{1:n}, \omega} \quad \sum_1^n \left[\ln\left\{\mathcal{N}\left(\boldsymbol{\mu}_{T_i}, \Sigma_{T_i}\right)\right\} + \ln\left\{\mathcal{N}\left(\boldsymbol{\mu}_{S_i}, \Sigma_{S_i}\right)\right\}\right] \quad (25)$$

Note that the densities $\mathcal{N}\left(\boldsymbol{\mu}_{T_i}, \Sigma_{T_i}\right)$ and $\mathcal{N}\left(\boldsymbol{\mu}_{S_i}, \Sigma_{S_i}\right)$ may be written as

$$\mathcal{N}\left(\boldsymbol{\mu}_{T_i}, \Sigma_{T_i}\right) = \frac{1}{\sqrt{|2\pi\Sigma_{T_i}|}} \exp\left\{ -\frac{1}{2}\left(\widehat{T}_i - \boldsymbol{\mu}_{T_i}\right)^T \Sigma_{T_i}^{-1}\left(\widehat{T}_i - \boldsymbol{\mu}_{T_i}\right)\right\} \quad (26)$$

where

$$\boldsymbol{\mu}_{T_i} = \begin{bmatrix}\phi_i \\ r_i \\ \omega\end{bmatrix} = \begin{bmatrix}\arctan 2\left(T_y - S_{i_y}, T_x - S_{i_x}\right) \\ \sqrt{\left(T_x - S_{i_x}\right)^2 + \left(T_y - S_{i_y}\right)^2} \\ \omega\end{bmatrix} \quad \&$$

$$\Sigma_{T_i} = \begin{bmatrix}\sigma_\phi^2 & 0 & 0 \\ 0 & \sigma_r^2(T, S_i, \omega) & 0 \\ 0 & 0 & \sigma_\varphi^2\end{bmatrix}$$

and

$$\mathcal{N}\left(\boldsymbol{\mu}_{S_i}, \Sigma_{S_i}\right) = \frac{1}{\sqrt{|2\pi\Sigma_{S_i}|}} \exp\left\{ -\frac{1}{2}\left(\widehat{S}_i - \boldsymbol{\mu}_{S_i}\right)^T \Sigma_{S_i}^{-1}\left(\widehat{S}_i - \boldsymbol{\mu}_{S_i}\right)\right\} \quad (27)$$

where

$$\boldsymbol{\mu}_{S_i} = \begin{bmatrix}S_{i_x} \\ S_{i_y}\end{bmatrix} \quad \& \quad \Sigma_{T_i} = \begin{bmatrix}\sigma_{i_x}^2 & 0 \\ 0 & \sigma_{i_y}^2\end{bmatrix}$$

After substituting (26) and (27) into (25), the maximum likelihood criteria may be written as

$$\begin{aligned} \min_{T, \mathbf{S}_{1:n}, \omega} \quad \sum_1^n \Bigg[& \frac{1}{2}\left(\widehat{T}_i - \boldsymbol{\mu}_{T_i}\right)^T \Sigma_{T_i}^{-1}\left(\widehat{T}_i - \boldsymbol{\mu}_{T_i}\right) + \\ & \frac{1}{2}\left(\widehat{S}_i - \boldsymbol{\mu}_{S_i}\right)^T \Sigma_{S_i}^{-1}\left(\widehat{S}_i - \boldsymbol{\mu}_{S_i}\right) + \\ & \ln\left\{\sqrt{|2\pi\Sigma_{T_i}|}\right\} + \ln\left\{\sqrt{|2\pi\Sigma_{S_i}|}\right\}\Bigg] \end{aligned} \quad (28)$$

Note that the term, $\ln\left\{\sqrt{|2\pi\Sigma_{T_i}|}\right\}$, in above equation is present due to the fact that Σ_{T_i} is a function of T, $\mathbf{S}$, and ω. The last term, $\ln\left\{\sqrt{|2\pi\Sigma_{S_i}|}\right\}$ can be ignored since Σ_{S_i} is a known constant matrix. Since Σ_{T_i} is assumed to be a diagonal matrix, (28) can be rewritten as

$$\begin{aligned} \min_{T, \mathbf{S}_{1:n}, \omega} \quad \sum_1^n \Bigg[& \ln(\varepsilon\sigma_r) + \frac{1}{2}\left(\widehat{T}_i - \boldsymbol{\mu}_{T_i}\right)^T \Sigma_{T_i}^{-1}\left(\widehat{T}_i - \boldsymbol{\mu}_{T_i}\right) \\ & + \frac{1}{2}\left(\widehat{S}_i - \boldsymbol{\mu}_{S_i}\right)^T \Sigma_{S_i}^{-1}\left(\widehat{S}_i - \boldsymbol{\mu}_{S_i}\right)\Bigg] \end{aligned} \quad (29)$$

where ε is defined as

$$\varepsilon = (2\pi)^{3/2}\sigma_\phi\sigma_\varphi$$

Apart from the initial term, $\ln(\varepsilon\sigma_r)$, the optimization problem given in (29) is similar to that used in the weighted nonlinear least-squares. Thus, the maximum likelihood approach presented here is similar to the weighted nonlinear least-squares estimation.

V. Nonlinear Least Squares

There exist no closed form solution to the nonlinear least-squares optimization problem given in (29) and therefore a numerical approach needs to be used. A few common approaches to solving the nonlinear least-squares problem include the Gauss-Newton method, Nelder-Mead simplex method, and Marquardt method [12]. Almost all these approaches are iterative methods that require an initial approximation to the unknown parameters and provide successively better approximations. The iterative process is repeated until the parameters do not change to within specified limits.

This section provides the Gauss-Newton method for solving the nonlinear least squares problem given in (29). The main advantage of the Gauss-Newton method is that it exhibits a "quadratic convergence," which, simply put, means that the uncertainty in the parameters after $p + 1$ iterations is proportional to the square of the uncertainty after p iterations. Once these uncertainties begin to get small, they decrease quite rapidly. An additional advantage of the Gauss-Newton method is that it only requires calculating the first-order derivatives. The major problem with the Gauss-Newton method is that it sometimes diverges if the initial approximation is too far from truth.

In order to simplify the formulation, we treat Σ_{T_i} as a known constant matrix. Thus, (29) can be rewritten as

$$\min_{T,\mathbf{S}_{1:n},\omega} \quad J = \frac{1}{2}\triangle\mathbf{y}^T W \triangle\mathbf{y} \tag{30}$$

where

$$\triangle\mathbf{y} = \begin{bmatrix} \widehat{T}_1 - \boldsymbol{\mu}_{T_1} \\ \widehat{S}_1 - \boldsymbol{\mu}_{S_1} \\ \vdots \\ \widehat{T}_n - \boldsymbol{\mu}_{T_n} \\ \widehat{S}_n - \boldsymbol{\mu}_{S_n} \end{bmatrix}, W = \begin{bmatrix} \Sigma_{T_i}^{-1} & 0 & 0 & 0 & 0 \\ 0 & \Sigma_{S_i}^{-1} & 0 & 0 & 0 \\ 0 & 0 & \ddots & 0 & 0 \\ 0 & 0 & 0 & \Sigma_{T_n}^{-1} & 0 \\ 0 & 0 & 0 & 0 & \Sigma_{S_n}^{-1} \end{bmatrix}$$

Let $\mathbf{x} = \begin{bmatrix} T_x & T_y & \omega & S_{1_x} & S_{1_y} & \dots & S_{n_x} & S_{n_y} \end{bmatrix}^T$ denote the parameters to be estimated and let $\mathbf{y} = \begin{bmatrix} \mathbf{f}_1^T(\mathbf{x}) & \dots & \mathbf{f}_i^T(\mathbf{x}) & \dots & \mathbf{f}_n^T(\mathbf{x}) \end{bmatrix}^T$ denote the measurements. Here $\mathbf{f}_i(\mathbf{x}) = \begin{bmatrix} \phi_i & r_i & \omega & S_{i_x} & S_{i_y} \end{bmatrix}^T$ is defined as

$$\mathbf{f}_i(\mathbf{x}) = \begin{bmatrix} \arctan 2\left(T_y - S_{i_y}, T_x - S_{i_x}\right) \\ \sqrt{\left(T_x - S_{i_x}\right)^2 + \left(T_y - S_{i_y}\right)^2} \\ \omega \\ S_{i_x} \\ S_{i_y} \end{bmatrix} \tag{31}$$

Also let $\widehat{\mathbf{y}} = \begin{bmatrix} \widehat{\mathbf{y}}_1^T, \dots, \widehat{\mathbf{y}}_i^T, \dots, \widehat{\mathbf{y}}_n^T \end{bmatrix}^T$ where $\widehat{\mathbf{y}}_i = \begin{bmatrix} \widehat{T}_i^T & \widehat{S}_i^T \end{bmatrix}^T$. Now $\triangle\mathbf{y}$ is defined as

$$\triangle\mathbf{y} = \widehat{\mathbf{y}} - \mathbf{y}$$

Let the *current* estimates estimates of $\mathbf{x}$ be denoted as

$$\mathbf{x}^c = \begin{bmatrix} T_x^c & T_y^c & \omega^c & S_{1_x}^c & S_{1_y}^c & \dots & S_{n_x}^c & S_{n_y}^c \end{bmatrix}^T$$

Define

$$\triangle\mathbf{x} = \mathbf{x} - \mathbf{x}^c$$

If the components of $\triangle\mathbf{x}$ are sufficiently small, then using the first-order Taylor series approximation, we have

$$\mathbf{f}(\mathbf{x}) \approx \mathbf{f}(\mathbf{x}^c) + F\triangle\mathbf{x} \tag{32}$$

where

$$F \equiv \left.\frac{\partial \mathbf{f}}{\partial \mathbf{x}}\right|_{\mathbf{x}^c}$$

Now the measurement residual $\triangle\mathbf{y}$ can be linearly approximated as

$$\triangle\mathbf{y} \approx \widehat{\mathbf{y}} - \mathbf{f}(\mathbf{x}^c) - F\triangle\mathbf{x} = \triangle\mathbf{y}^c - F\triangle\mathbf{x} \tag{33}$$

where $\triangle\mathbf{y}^c = \widehat{\mathbf{y}} - \mathbf{f}(\mathbf{x}^c)$. Substituting (33) in (30) yields

$$J \approx \frac{1}{2}\left(\triangle\mathbf{y}^c - F\triangle\mathbf{x}\right)^T W \left(\triangle\mathbf{y}^c - F\triangle\mathbf{x}\right) \tag{34}$$

The $\triangle\mathbf{x}$ that minimizes the above cost function can be written as

$$\triangle\mathbf{x} = \left(F^T W F\right)^{-1} F^T W \triangle\mathbf{y}^c \tag{35}$$

After obtaining $\triangle\mathbf{x}$, the current estimates are redefined as

$$\mathbf{x}^c = \triangle\mathbf{x} + \mathbf{x}^c \tag{36}$$

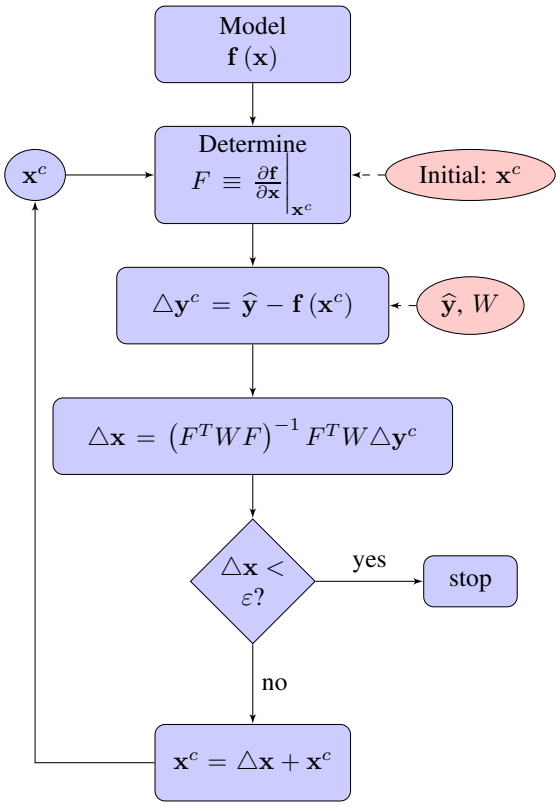

Figure 3. Gauss-Newton Algorithm.

Now using the current estimates, F, W, and $\triangle\mathbf{y}^c$ are calculated. Then, $\triangle\mathbf{x}$ estimate for the next iteration is calculated from (35) and this process is repeated until $\triangle\mathbf{x}$ converges to a prescribed small value. A schematic representation of the Gauss-Newton algorithm is presented in figure 3.

VI. Results

This section presents numerical simulations to assess the localization improvement due to the proposed fusion algorithm. Here we consider two separate simulation scenarios, for both scenarios, we assume that there are five sensor nodes located at

$$\mathbf{S} = \begin{bmatrix} 127 & 20 & 90 & 136 & 182 \\ 107 & 22 & 0 & 68 & 59 \end{bmatrix}$$

For simulation purposes, we assume a constant velocity model for the bullet. Thus, the Mach number is selected to be $m = 2$ and the speed of sound is selected to be $c = 342\ m/sec$. For both scenarios, the measurement noise models are selected as $\sigma_{i_x} = \sigma_{i_y} = 5m$, $\sigma_\phi = \sigma_\varphi = 4^o$, and $\sigma_\tau = 1\ msec$. Since there exist several approaches to solve the nonlinear least-squares problem, two different methods are used to obtain solutions for both simulation scenarios. In the first method, the optimization problem is solved using the Gauss-Newton method [12] presented in the previous section. The second approach uses the Nelder-Simplex algorithm [13], i.e., the *fminsearch* function in Matlab.

A. *Simulation I*

For the first simulation, the shooter is assumed to be located at $T = \begin{bmatrix} 50 & 50 \end{bmatrix}^T$ and we select the bullet trajectory to be $\omega = 30^o$. Figure 4 shows the first simulation scenario. Due to the sensor locations, the second and the third sensors do not receive the shockwave.

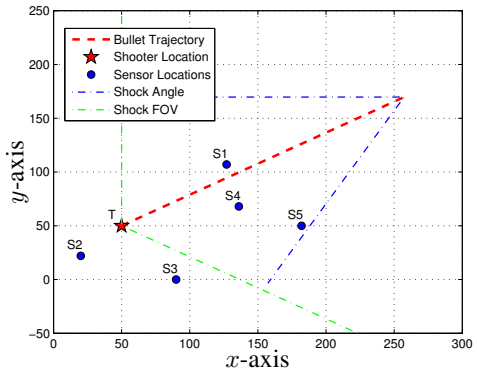

Figure 4. Simulation I Scenario

In order to evaluate the system performance, a Monte Carlo simulation is conducted for both the Gauss-Newton method and the simplex algorithm. The mean shooter locations and the associated error ellipses obtained from the Monte Carlo simulations using the Gauss-Newton method are given in figure 5. A separate plot is not provided for the results obtained using the simplex algorithm since they are very similar to that obtained for the Gauss-Newton method. Figure 5 indicates that the sensor five performs the worst out of the three sensors in the shockwave FOV. Figure 5 also indicates that the fused estimate is superior to the individual sensor estimates, and the uncertainty associated with the fused estimates is much less than the uncertainty associated with the individual sensor estimates.

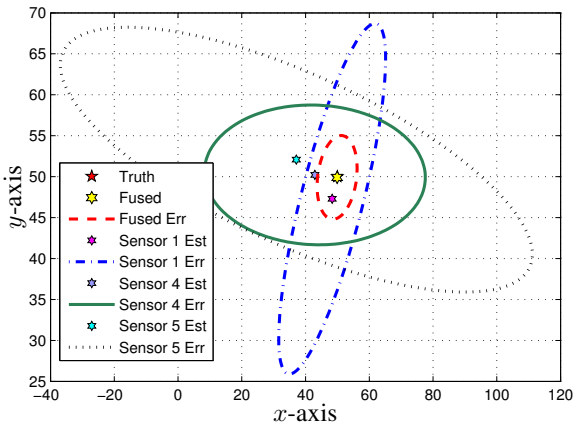

Figure 5. Simulation I: Mean Results from Monte Carlo Runs

Table I contains the mean shooter location estimate of the individual sensors and the fusion algorithms over the Monte Carlo run. The "average" estimate presented in table I indicates the estimate obtained by simply averaging the individual target estimate from sensors one, four, and five. Table I also contains the root mean square error (RMSE) associated with each estimate. Based on the RMSE presented in table I, one could conclude that that fused estimates outperform the individual sensors and the simple average estimate.

Table I
SIMULATION I: SHOOTER LOCATION

	T_x (m)	T_y (m)	RMSE (m)
Truth	50	50	–
Sensor 1	48.3513	47.2948	23.2870
Sensor 2	–	–	–
Sensor 3	–	–	–
Sensor 4	42.9248	50.2141	31.1132
Sensor 5	37.1197	52.0782	65.6542
Average	42.7986	49.8623	25.9660
Gauss-Newton	49.9066	49.9134	6.8639
Nedler-Simplex	50.0493	50.0588	6.9972

Table II contains the mean bullet trajectory angle estimate obtained from the individual sensors and the fusion algorithms over the Monte Carlo run. Table II also contains the RMSE associated with each trajectory angle estimate. Note that the fused trajectory estimate is simply the average of the individual sensor estimates due to the way in which ω appears in (31).

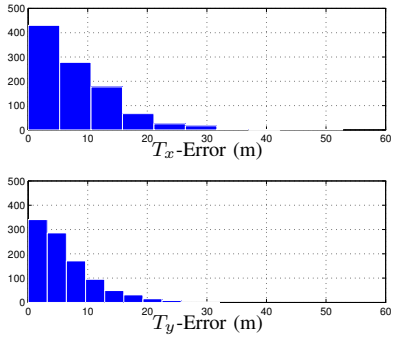

Figure 6. Simulation I: Localization error histogram for average estimates

Figure 6 presents the shooter localization error histogram for the average estimate, i.e., the estimate obtained by simply averaging the individual target estimates from sensors one, four, and five. Figure 7 presents the localization error histogram for the fused estimate obtained for the Gauss-Newton method.

Table III contains RMSE associated with the sensor location estimates. Interestingly, the fusion algorithm was able to improve the sensor location accuracy by reducing the GPS uncertainties. Based on the RMSE presented in tables I,II, and III, one could conclude that that fused estimates outperform the individual sensors.

B. *Simulation II*

For the second simulation, the shooter is assumed to be located at $T = \begin{bmatrix} 150 & -50 \end{bmatrix}^T$ and we select the bullet

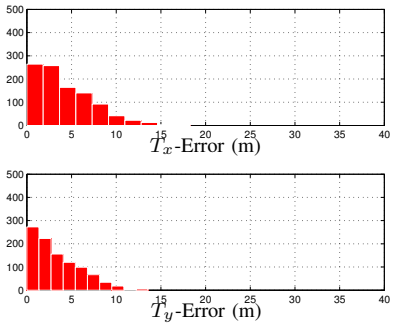

Figure 7. Simulation I: Localization error histogram for fused estimates

Table II
SIMULATION I: BULLET TRAJECTORY

	ω (deg)	RMSE (deg)
Truth	30	–
Sensor 1	30.0641	3.9690
Sensor 2	–	–
Sensor 3	–	–
Sensor 4	30.3402	3.9970
Sensor 5	29.9591	3.9029
Average	30.1211	2.2128
Gauss-Newton	30.1211	2.2128
Nedler-Simplex	30.1999	2.4674

Table III
SIMULATION I: SENSOR LOCATION RMSE

	GPS (m)	Gauss-Newton (m)	Nedler-Simplex (m)
Sensor 1	7.0215	6.5453	6.5938
Sensor 2	7.0002	6.3195	6.3530
Sensor 3	7.0028	6.6513	6.6770
Sensor 4	7.1509	6.5259	6.6201
Sensor 5	7.0223	6.7883	6.8731

trajectory to be $\omega = 170^o$. Figure 8 shows scenario for the second simulation. As shown in figure 8, only the second and the third sensors are in the FOV of the shockwave.

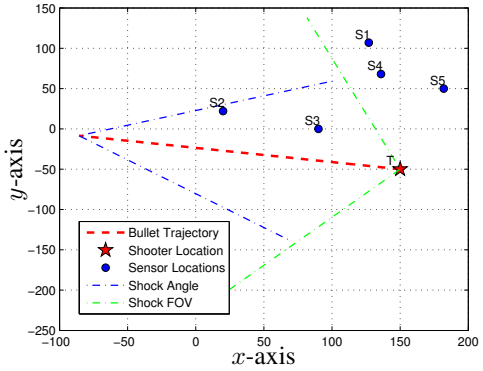

Figure 8. Simulation II Scenario

The mean shooter locations and the associated error ellipses obtained from the Monte Carlo simulation using the Gauss-Newton method are given in figure 9. Figure 9 indicates that both sensor two and sensor three are of similar accuracy since they are equal distance from the bullet trajectory. Figure 9 also indicates that the fused estimate is superior to individual sensor estimates and the uncertainty associated with the fused estimates is much less than the uncertainty associated with the individual sensor estimates.

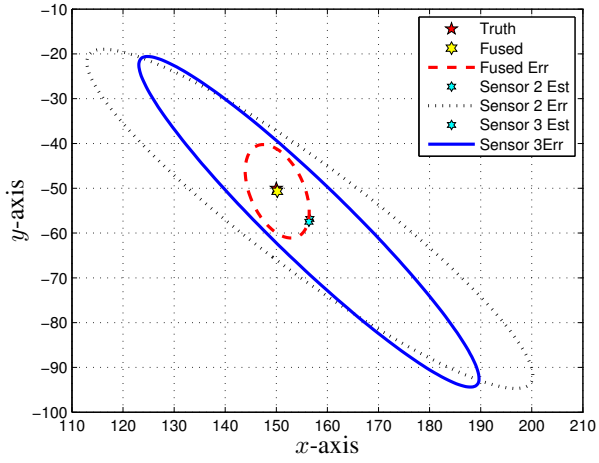

Figure 9. Simulation II: Mean Results from Monte Carlo Runs

Table IV contains the mean shooter location estimate of the individual sensors and the fusion algorithms over the Monte Carlo runs. Table IV also contains the RMSE associated with each estimate. Based on the RMSE presented in table IV, one could conclude that that fused estimates outperform the individual sensors and the simple average estimate.

Table IV
SIMULATION II: SHOOTER LOCATION

	T_x (m)	T_y (m)	RMSE (m)
Truth	150	-50	–
Sensor 1	–	–	–
Sensor 2	156.5714	-56.8403	49.9558
Sensor 3	156.3943	-57.4820	43.3278
Sensor 4	–	–	–
Sensor 5	–	–	–
Average	156.4828	-57.1611	34.2454
Gauss-Newton	150.1808	-50.6793	10.3593
Nedler-Simplex	150.0338	-50.5054	10.7630

Figure 10 presents the shooter localization error histogram for the average estimate and figure 11 presents the localization error histogram for the fused estimate obtained for the Gauss-Newton method.

Table V contains the mean bullet trajectory angle estimate and associated RMSE obtained from the individual sensors and the fusion algorithms over the Monte Carlo runs. Finally, table VI contains RMSE associated with the sensor location estimates for simulation two. Note that the fusion algorithm was able to improve the sensor location accuracy by reducing the GPS uncertainties. The RMSE presented in tables IV,V, and VI, indicate that fused estimates outperform the individual sensors for the second simulation.

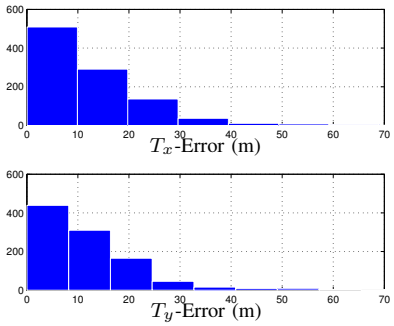

Figure 10. Simulation II: Localization error histogram for average estimates

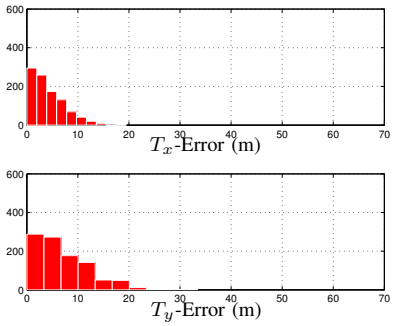

Figure 11. Simulation II: Localization error histogram for fused estimates

Table V
SIMULATION II: BULLET TRAJECTORY

	ω (deg)	RMSE (deg)
Truth	170	–
Sensor 1	–	–
Sensor 2	169.8829	4.1206
Sensor 3	169.9445	4.0493
Sensor 4	–	–
Sensor 5	–	–
Average	169.9137	2.8139
Gauss-Newton	169.9137	2.8139
Nedler-Simplex	169.9098	3.0287

Table VI
SIMULATION II: SENSOR LOCATION RMSE

	GPS (m)	Gauss-Newton (m)	Nedler-Simplex (m)
Sensor 1	6.9913	6.7276	6.7284
Sensor 2	6.9897	6.7586	6.7848
Sensor 3	6.9484	6.6360	6.6923
Sensor 4	7.0946	6.7296	6.7282
Sensor 5	7.0078	6.7280	6.7317

VII. FINAL REMARKS

The shooter localization problem using a network of soldier-worn gunfire detection systems is considered here. This paper presents a fusion algorithm that utilizes the benefits of the sensor network layout of all the sensors within a small combat unit to help refine the shooter localization accuracy. The individual gunfire detection systems considered here are composed of a passive array of microphones that is able to localize a gunfire event by measuring the direction of arrival for both the muzzle blast and the shockwave. After detecting a gunfire, the individual sensors report their solution along with their GPS positions to a central fusion node. At the central node, the individual solutions are fused along with the GPS locations on the soldiers to yield a highly accurate geo-rectified solution. Numerical results given here indicate that the fused estimates are more accurate than the individual localization results. Future work include further analyzing the linearization issues associated with the maximum likelihood approach and developing a mathematically rigorous method to quantify the uncertainties associated with the maximum likelihood estimates.

ACKNOWLEDGEMENT

This work is conducted in collaboration with the US Army Natick Soldier Research Development & Engineering Center (NSRDEC) and the US Army Armament Research, Development and Engineering Center (ARDEC).

REFERENCES

[1] G. L. Duckworth, D. C. Gilbert, and J. E. Barger, "Acoustic counter-sniper system," in *Society of Photo-Optical Instrumentation Engineers (SPIE) Conference Series*, ser. Presented at the Society of Photo-Optical Instrumentation Engineers (SPIE) Conference, D. Spector & E. M. Carapezza, Ed., vol. 2938, Feb. 1997, pp. 262–275.

[2] J. Bedard and S. Pare, "Ferret: a small arms fire detection system: localization concepts," vol. 5071, no. 1. SPIE, 2003, pp. 497–509.

[3] J. Millet and B. Balingand, "Latest achievements in gunfire detection systems," in *In Proc. RTO MP-SET-107 Battlefield Acoustic Sensing for ISR Applications*, Oct. 2006.

[4] J. Ash, G. Whipps, and R. Kozick, "Performance of shockwave-based shooter localization under model misspecification," in *Acoustics Speech and Signal Processing (ICASSP), 2010 IEEE International Conference on*, 2010, pp. 2694 – 2697.

[5] P. Kuckertz, J. Ansari, J. Riihijarvi, and P. Mahonen, "Sniper fire localization using wireless sensor networks and genetic algorithm based data fusion," in *Military Communications Conference, 2007. MILCOM 2007. IEEE*, 2007, pp. 1 – 8.

[6] M. Maroti, G. Simon, A. Ledeczi, and J. Sztipanovits, "Shooter localization in urban terrain," *Computer*, vol. 37, no. 8, pp. 60 – 61, 2004.

[7] L. Kaplan, T. Damarla, and T. Pham, "QoI for passive acoustic gunfire localization," in *Mobile Ad Hoc and Sensor Systems, 2008. MASS 2008. 5th IEEE International Conference on*, Oct. 2008, pp. 754 –759.

[8] A. Ledeczi, P. Volgyesi, M. Maroti, G. Simon, G. Balogh, A. Nadas, B. Kusy, S. Dora, and G. Pap, "Multiple simultaneous acoustic source localization in urban terrain," in *In Proc. 4th International Symposium on Information Processing in Sensor Networks (IPSN*, 2005.

[9] P. Volgyesi, G. Balogh, A. Nadas, C. B. Nash, A. Ledeczi, K. Pence, T. Bapty, J. Scott, and T. N. Police, "Shooter localization and weapon classification with soldier-wearable networked sensors," in *Conference on Mobile Systems, Applications, and Services*, 2007.

[10] D. Lindgren, O. Wilsson, F. Gustafsson, and H. Habberstad, "Shooter localization in wireless sensor networks," in *Information Fusion, 2009. FUSION '09. 12th International Conference on*, 2009, pp. 404 –411.

[11] R. Kozick, G. Whipps, and B. Sadler, "Accuracy and tradeoff analysis of sniper localization systems with a network of acoustic sensors," in *in Proc. MSS Battlespace Acoustics & Seismic Sensing, Magnetic & Electric Field Sensors*, 2009.

[12] J. L. Crassidis and J. L. Junkins, *Optimal Estimation of Dynamic System*. Boca Raton, FL: Chapman & Hall/CRC, 2004, ch. 1.

[13] J. A. Nelder and R. Mead, "A Simplex Method for Function Minimization," *The Computer Journal*, vol. 7, no. 4, pp. 308–313, 1965.